



Efficient Aggregation-Induced Delayed Fluorescence Luminogens for Solution-Processed OLEDs With Small Efficiency Roll-Off

Zheyi Cai¹, Hao Chen¹, Jingjing Guo¹, Zujin Zhao^{1*} and Ben Zhong Tang^{1,2*}

¹ State Key Laboratory of Luminescent Materials and Devices, Guangdong Provincial Key Laboratory of Luminescence From Molecular Aggregates, Guangzhou, China, ² Department of Chemistry, Hong Kong Branch of Chinese National Engineering Research Center for Tissue Restoration and Reconstruction, The Hong Kong University of Science and Technology, Kowloon, China

OPEN ACCESS

Edited by:

Guohua Xie,
Wuhan University, China

Reviewed by:

Yanqin Miao,
Taiyuan University of
Technology, China
Dongxia Zhu,
Northeast Normal University, China

*Correspondence:

Zujin Zhao
mszjzhao@scut.edu.cn
Ben Zhong Tang
tangbenz@ust.hk

Specialty section:

This article was submitted to
Organic Chemistry,
a section of the journal
Frontiers in Chemistry

Received: 24 January 2020

Accepted: 02 March 2020

Published: 07 April 2020

Citation:

Cai Z, Chen H, Guo J, Zhao Z and
Tang BZ (2020) Efficient
Aggregation-Induced Delayed
Fluorescence Luminogens for
Solution-Processed OLEDs With
Small Efficiency Roll-Off.
Front. Chem. 8:193.
doi: 10.3389/fchem.2020.00193

Purely organic small molecules with thermally-activated delayed fluorescence have a high potential for application in organic light-emitting diodes (OLEDs), but overcoming severe efficiency roll-off at high voltages still remains challenging. In this work, we design and synthesize two new emitters consisting of electron-withdrawing benzoyl and electron-donating phenoxazine and 9,9-dihexylfluorene. Their electronic structures, thermal stability, electrochemical behaviors, photoluminescence property, and electroluminescence performance are thoroughly investigated. These new emitters show weak fluorescence in dilute solution, but they can emit strongly with prominent delayed fluorescence in the aggregated state, indicating the aggregation-induced delayed fluorescence (AIDF) character. The solution-processed OLEDs based on the two emitters show high external quantum efficiency of 14.69%, and the vacuum-deposited OLEDs can also provide comparable external quantum efficiency of 14.86%. Significantly, roll-offs of the external quantum efficiencies are very small (down to 0.2% at 1,000 cd m⁻²) for these devices, demonstrating the evidently advanced efficiency stability. These results prove that the purely organic emitters with AIDF properties can be promising to fabricate high-performance solution-processed OLEDs.

Keywords: aggregation-induced delayed fluorescence, thermally activated delayed fluorescence, electroluminescence, organic light-emitting diodes, efficiency roll-off

INTRODUCTION

Organic light-emitting diodes (OLEDs) are attracting considerable attention across academia and industry because of their advantages of flexibility, fast response, high stability, light weight, and so forth. Generally, for conventional fluorescent organic materials, the ratio of electrically generated singlet and triplet excitons is 1:3, leading to a low internal quantum efficiency (IQE) limited to only 25%. One way to enhance the IQE is making full use of triplet excitons. As for phosphorescent materials, the theoretical maximum value of the IQE can reach 100%, resulting from utilizing both triplet and singlet excitons, but most of these materials have to incorporate precious heavy metals to promote intersystem crossing (ISC). The OLEDs based on such materials have high costs in noble metals, and often encounter aggregation or concentration caused emission quenching. Another way to enhance the IQE of purely organic materials is transforming triplet excitons to singlet excitons.

According to the reports in recent years, there are several strategies to make use of the non-radiative triplet excitons, and thermally activated delayed fluorescence (TADF) is the method with most potential, in which triplet excitons can be converted to singlet excitons via reverse intersystem crossing (RISC) due to small singlet–triplet energy gap (ΔE_{ST}) (Gong et al., 2011; Uoyama et al., 2012; Hirata et al., 2015; Kang et al., 2018). TADF materials are able to harvest both singlet and triplet excitons and thus can reach high exciton utilization without noble metal, but suffer from severe efficiency roll-off (Rajamalli et al., 2016, 2017; Xie et al., 2017). Recently, by taking the advantages of aggregation-induced emission (AIE) and TADF, a new molecular design strategy of aggregation-induced delayed fluorescence (AIDF) was proposed and a series of novel luminogens based on AIDF were developed. These AIDF materials could not only harness both singlet and triplet excitons, but also showed the merit of very small efficiency roll-off at high luminance (Huang et al., 2017; Guo et al., 2018, 2019).

On the other hand, compared to vacuum deposition, solution-processed film preparation techniques, including spin-coating, inkjet printing, roll to roll processing, etc., are fitter to manufacture large-area OLED devices with lower cost and less material waste (Gather et al., 2011; Gong et al., 2013; Cho et al., 2014; Albrecht et al., 2015; Zeng et al., 2019). Currently, luminescent polymers are the major choice to fabricate solution-processed devices due to their excellent film-forming ability (Lee et al., 2016; Shao et al., 2017; Kim et al., 2018; Zou et al., 2018). However, it is generally hard to remove the metal catalyst residue completely from the products, and as a result they are in low purity and have defects in many cases, which undermine their EL performance. Meanwhile, the reproducibility is another problem for the polymers. In opposition, small molecules have the advantages of clearly defined structures, easy purification, and better photoluminescence (PL) performance. So, in addition to conventional fluorescent and phosphorescent small molecules (Zhao et al., 2007, 2009; Yang et al., 2018), developing solution-processable small molecules with delayed fluorescence is of high significance. However, the currently reported solution-processable TADF molecules also suffer from severe efficiency roll-off at high voltages (Wu et al., 2009; Suzuki et al., 2015; Zhong et al., 2020). To solve this problem, in this work, we designed and synthesized two small molecules with AIDF property. Long alkyl chains are introduced into the molecules to enhance the film-forming ability for solution-processed OLED devices. They emit strong yellow to orange-yellow light with evident delayed fluorescence in solid film. The solution-processed OLEDs using them as emitting layers exhibit high EL efficiencies and very small efficiency roll-off.

EXPERIMENTAL

Synthesis

9,9-Dihexyl-9H-fluorene (1)

Potassium *tert*-butoxide (16.83 g, 150 mmol) was added to a mixture of fluorene (8.30 g, 50 mmol) and 1-bromohexane (17.45 mL, 125 mmol) in dehydrated tetrahydrofuran (100 mL) and stirred for 12 h under 65°C. The reaction mixture was poured

into water and extracted with dichloromethane several times. The combined organic layers were washed with water twice, and then dried over anhydrous NaSO₄. After filtration, the crude product was concentrated and purified by column chromatography on silica gel (petroleum ether) to afford **1** as colorless liquid in 97% yield (16.21 g). ¹H NMR (500 MHz, CDCl₃) δ (TMS, ppm): 7.70–7.65 (m, 2H), 7.33–7.23 (m, 6H), 1.99–1.92 (m, 4H), 1.13–0.98 (m, 12H), 0.74 (t, $J = 7.2$ Hz, 6H), 0.67–0.54 (m, 4H). ¹³C NMR (125 MHz, CDCl₃) δ (TMS, ppm): 150.65, 141.12, 126.97, 126.76, 122.79, 119.62, 55.12, 39.69, 32.17, 29.75, 23.57, 22.49, 13.99.

(9,9-Dihexyl-9H-fluorene-2-yl)(4-fluorophenyl)Methanone (2a) and (9,9-dihexyl-9H-fluorene-2,7-diyl)bis(4-fluorophenyl)Methanone (2b)

Aluminum trichloride (12.00 g, 90 mmol) was added into a stirred solution of **1** (9.70 g, 29 mmol) and 4-fluorobenzoyl chloride (14.22 g, 90 mmol) in dehydrated dichloromethane (50 mL) in 45°C and stirred for 6 h. The reaction was quenched with ice water and hydrochloric acid (50 mL, 2:1 v/v), and extracted with dichloromethane several times. The combined organic layers were washed with water twice, and then dried over anhydrous NaSO₄. After filtration and solvent evaporation under reduced pressure, the residue was purified by column chromatography on silica gel (dichloromethane: petroleum ether, 2:3 v/v) to afford **2a** as yellow solid in 50% yield (6.61 g) and **2b** as yellow solid in 18% yield (3.02 g). For **2a**, ¹H NMR (500 MHz, CD₂Cl₂) δ (TMS, ppm): 7.83–7.75 (m, 4H), 7.71–7.64 (m, 4H), 7.44–7.32 (m, 3H), 2.05–1.97 (m, 4H), 1.16–0.98 (m, 12H), 0.76 (t, $J = 7.2$ Hz, 6H), 0.66–0.56 (m, 4H). ¹³C NMR (125 MHz, CD₂Cl₂) δ (TMS, ppm): 196.66, 153.28, 152.12, 147.08, 141.11, 138.51, 136.91, 132.80, 132.77, 130.91, 129.74, 128.35, 128.19, 125.84, 124.46, 121.96, 120.65, 56.63, 41.38, 32.81, 30.90, 25.10, 23.84, 15.05, 0.90. For **2b**, ¹H NMR (500 MHz, CDCl₃) δ (TMS, ppm): 7.91–7.84 (m, 6H), 7.83–7.79 (m, 4H), 7.23–7.16 (m, 4H), 2.06–1.99 (m, 4H), 1.17–1.01 (m, 12H), 0.78 (t, $J = 7.2$ Hz, 6H), 0.70–0.60 (m, 4H). ¹³C NMR (125 MHz, CDCl₃) δ (TMS, ppm): 198.49, 168.36, 164.38, 151.96, 144.94, 137.63, 134.25, 132.74, 129.80, 125.55, 119.88, 114.74, 113.69, 57.91, 39.34, 32.03, 29.55, 23.93, 22.55, 15.40.

((4-(10H-Phenoxazin-10-yl)phenyl)(9,9-dihexyl-9H-fluorene-2-yl)methanone) (FC6-BP-PXZ)

A mixture of **2a** (0.46 g, 1.0 mmol), phenoxazine (0.24 g, 1.3 mmol) and potassium *tert*-butoxide (0.23 g, 2.0 mmol) in deaerated *N,N*-dimethylformamide (20 mL) was heated up to 130°C and stirred for 12 h under nitrogen. After cooling down to room temperature, the reaction was quenched with water (20 mL), and extracted with dichloromethane several times. The combined organic layers were washed with water twice, and then dried over anhydrous NaSO₄. After filtration and solvent evaporation under reduced pressure, the residue was purified by column chromatography on silica gel (dichloromethane: petroleum ether, 1:1 v/v) to afford orange solid of FC6-BP-PXZ in 37% yield (0.23 g). ¹H NMR (500 MHz, CD₂Cl₂) δ (TMS, ppm): 8.05–8.02 (m, 2H), 7.90 (s, 1H), 7.86–7.79 (m, 3H), 7.54–7.49 (m, 2H), 7.45–7.35 (m, 3H), 6.94–6.42 (m, 6H), 6.06 (s, 2H), 2.14–1.97 (m, 4H), 1.18–0.97 (m, 12H), 0.75 (t, $J = 7.1$ Hz, 6H),

0.70–0.57 (m, 4H). ^{13}C NMR (125 MHz, CD_2Cl_2) δ (TMS, ppm): 195.86, 153.14, 151.38, 146.89, 140.24, 139.06, 136.09, 133.05, 130.32, 127.48, 124.87, 123.61, 120.45, 119.25, 113.41, 56.84, 40.52, 31.93, 29.54, 24.25, 22.48, 15.73. HRMS ($\text{C}_{44}\text{H}_{45}\text{NO}_2$): m/z 619.1476 [M^+ , calcd 619.3450].

((9,9-Dihexyl-9H-fluorene-2,7-diyl)bis((4-(10H-phenoxazin-10-yl)phenyl)methanone)) (FC6-2BP-PXZ)

A mixture of **3b** (0.8674 g, 1.5 mmol), phenoxazine (0.8238 g, 4.5 mmol) and potassium *tert*-butoxide (0.5049 g, 4.5 mmol) in deaerated *N,N*-dimethylformamide (20 mL) was heated up to 130°C and stirred for 12 h under nitrogen. After cooling down to room temperature, the reaction was quenched with water (20 mL), and extracted with dichloromethane several times. The combined organic layers were washed with water twice, and then dried over anhydrous Na_2SO_4 . After filtration and solvent evaporation under reduced pressure, the residue was purified by column chromatography on silica gel (dichloromethane: petroleum ether, 1:1 v/v) to afford orange solid of FC6-2BP-PXZ in 66% yield (0.90 g). ^1H NMR (500 MHz, CD_2Cl_2) δ (TMS, ppm): 8.09–8.03 (m, 4H), 7.99–7.94 (m, 4H), 7.93–7.88 (m, 2H), 7.56–7.42 (m, 4H), 6.84–6.56 (m, 12H), 6.07 (s, 4H), 2.16–2.08 (m, 4H), 1.18–0.98 (m, 12H), 0.74 (t, $J = 7.0$ Hz, 6H), 0.72–0.65 (m, 4H). ^{13}C NMR (125 MHz, CDCl_3) δ (TMS, ppm): 195.56, 137.77, 136.80, 133.74, 130.82, 130.12, 123.29, 120.45, 115.75, 31.49, 23.98, 22.54, 13.97. HRMS ($\text{C}_{63}\text{H}_{56}\text{N}_2\text{O}_2$): m/z 904.1583 [M^+ , calcd 904.4240].

OLED Fabrication and Characterization

The solution-processed devices were fabricated on clean glass substrates pre-coated with a 180 nm-thin layer of indium tin oxide (ITO) with a sheet resistance of $10\ \Omega$ per square. The ITO surface was treated with an ultrasonic detergent bath for 90 min, followed by soaking in ultrasonic de-ionized water for 20 min, then dried at 120°C for 1 h, and UV/Ozone cleaning for 15 min before spin-coating. A 50 nm-thin poly(3,4-ethylenedioxythiophene):poly(styrenesulfonate) (PEDOT:PSS) layer was spin-coated onto ITO surface at 3,000 rpm, then baked at 150°C for 50 min to remove the residual water. Then, the substrates were moved into a glovebox under a nitrogen atmosphere, and a poly(9-vinylcarbazole) (PVK) layer was spin-coated onto the PEDOT:PSS layer at 2,500 rpm (the thickness achieved 30 nm) from a filtered $10\ \text{mg mL}^{-1}$ chlorobenzene solution, followed by drying at 120°C for 20 min. Then, the emitting layer was spin-coated according to the configuration requirement. Solutions of FC6-BP-PXZ (30 wt%) or FC6-2BP-PXZ (10 wt%) doped in 4,4'-bis(carbazol-9-yl)biphenyl (CBP) with an overall concentration of $20\ \text{mg mL}^{-1}$ in toluene were spin-coated at 2,500 rpm for 45 s to get films with a thickness of 50 nm. Finally, an electron-transport layer of 1,3,5-tri(*m*-pyrid-3-yl-phenyl)benzene (TmPyPB), a LiF layer, and an Al layer were deposited consecutively onto the spin-coated film in a vacuum chamber under 10^{-4} Pa. Vacuum-evaporation OLEDs were fabricated on clean glass substrates pre-coated with a 180-nm-thin layer of ITO with a sheet resistance of $10\ \Omega$ per square. Organic layers were deposited by high-vacuum ($5 \times$

10^{-4} Pa) thermal evaporation onto a glass substrate pre-coated with an ITO layer. All organic layers were deposited sequentially. Thermal deposition rates for the organic materials, LiF and Al were 0.5, 0.5, and $1\ \text{\AA s}^{-1}$, respectively. The thicknesses of the vacuum deposited layers were monitored by quartz crystal microbalance and were calibrated by Dektak XT profilometer. The emission area of the devices is $3 \times 3\ \text{mm}^2$ as shaped by the overlapping area of the anode and cathode. All the device characterization steps were carried out at room temperature under ambient laboratory conditions without encapsulation. EL spectra were taken by an optical analyzer, FLAME-S-VIS-NIR. Current density and luminance vs. driving voltage characteristics were measured by Keithley 2400 and Konica Minolta chromameter CS-200. External quantum efficiencies were calculated by assuming that the devices were Lambertian light sources.

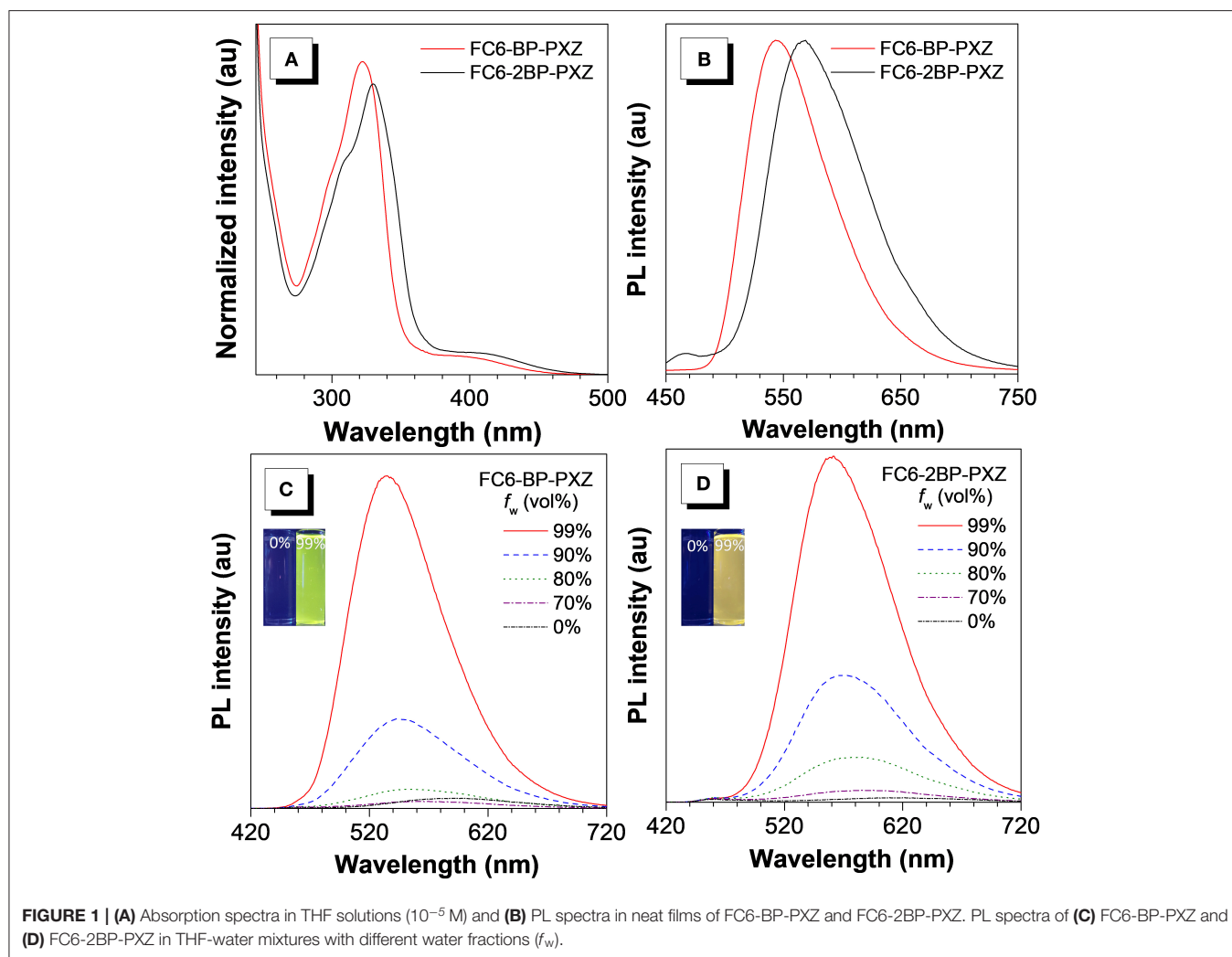
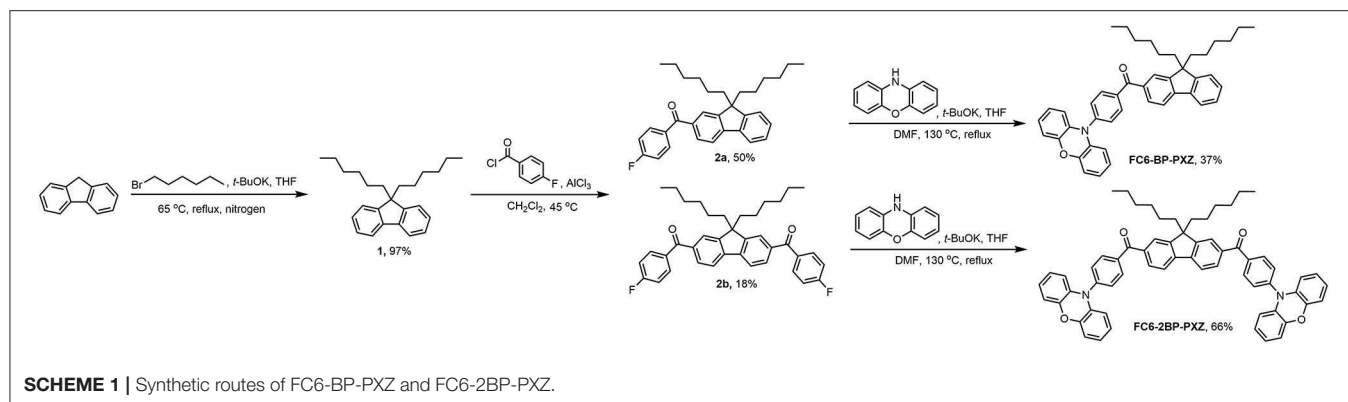
RESULTS AND DISCUSSION

Synthesis and Thermal Stability

The target compounds FC6-BP-PXZ and FC6-2BP-PXZ were simply and efficiently synthesized. As shown in **Scheme 1**, 9,9-dihexyl-9H-fluorene (**1**) that was prepared by the method in reported literature underwent Friedel-Crafts acylation reaction with compound **2** to yield intermediate **3a** and **3b**. The treatments of **3a** and **3b** with phenoxazine (PXZ) furnished the final compounds FC6-BP-PXZ and FC6-2BP-PXZ, respectively, in high yields. The molecular structures had been well-characterized by NMR and high-resolution mass spectra. Owing to the presence of hexyl groups, both compounds have good solubility in common organic solvents, such as chlorobenzene, toluene, chloroform, dichloromethane, tetrahydrofuran (THF), and so on, but do not dissolve easily in water because of the hydrophobic structures. The thermal stability of both compounds is characterized thoroughly by thermogravimetric analysis (TGA) and differential scanning calorimetry (DSC) under nitrogen. FC6-BP-PXZ and FC6-2BP-PXZ show high decomposition temperatures of 340.1 and 424.5°C , and high glass-transition temperatures of 85.7 and 84.0°C , respectively (**Figure S1**). The good thermal and morphological stabilities of both compounds enable them to function in OLEDs, and benefit device performances.

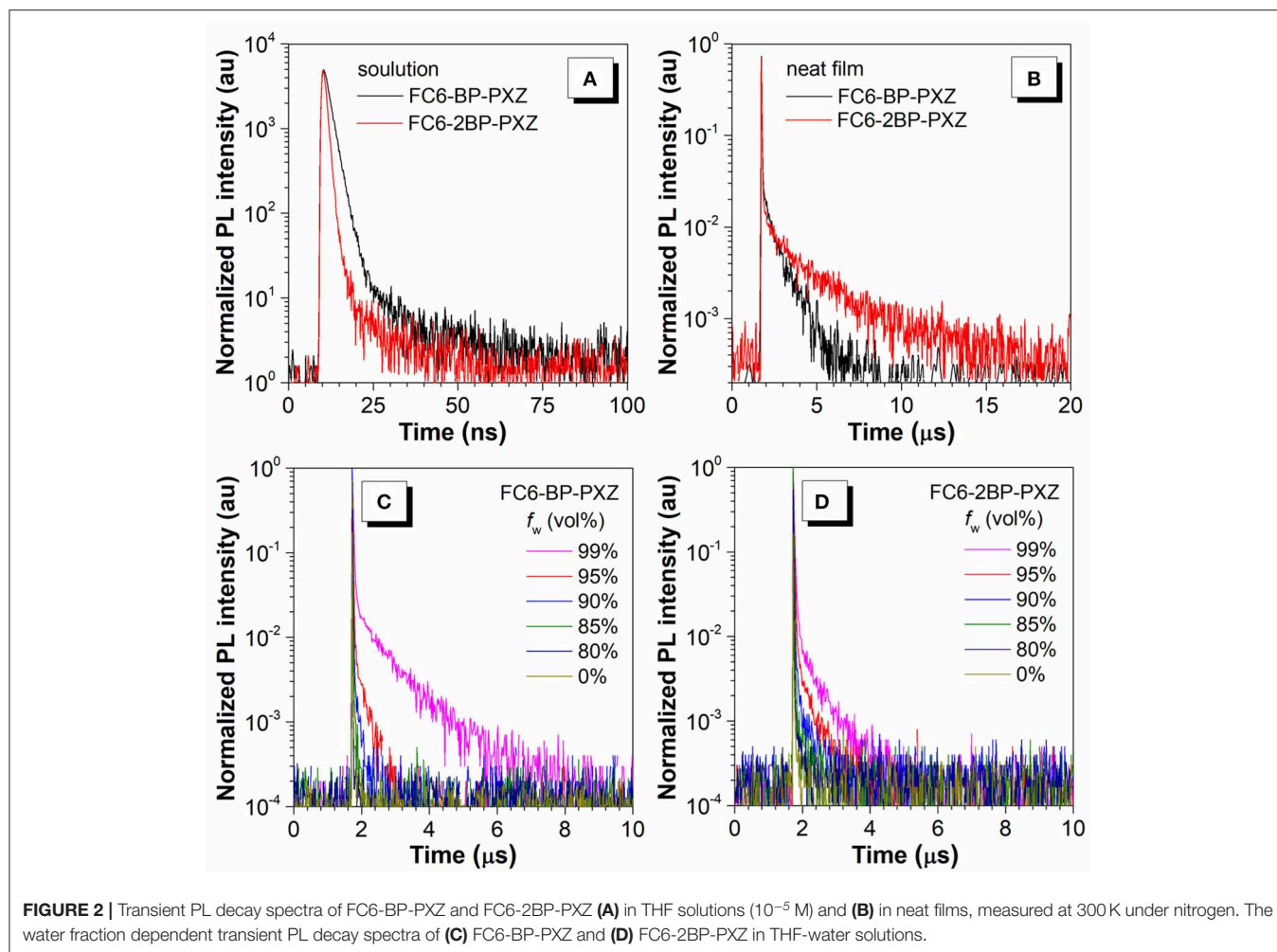
Photophysical Behavior

FC6-BP-PXZ and FC6-2BP-PXZ show strong absorption bands at around 317 and 330 nm in THF solution, associated with π - π^* transition of the molecules. There are also weak absorption bands at around 400 nm resulting from twisted intramolecular charge transfer (TICT) from the electronic donating-accepting (D-A) structure (**Figure 1A**) (Kashihara et al., 2017; Thorat et al., 2017; Higginbotham et al., 2018). In THF solution, FC6-BP-PXZ and FC6-2BP-PXZ emit weakly at 543 and 550 nm, with low fluorescence quantum yields (Φ_{FS}) of 3.5 and 2.0%, (**Figure 2A**) respectively. However, they can emit strongly at 544 and 567 nm with higher Φ_{FS} of 32.0 and 17.0% in neat films at 300 K, respectively, indicating they have AIE property (**Figures 1B, 2B**



and Table S2). To further confirm this, the PL behaviors are measured in their water-THF mixtures (Figures 1C,D). The emission intensity is much stronger and the emission peak is blue-shifted when water fraction in the mixture gets high. Since these compounds are insoluble in water, they are prone to form aggregates when the water fraction becomes high, indicating

the enhanced emission is caused by the aggregate formation. In the aggregated state, the intramolecular motions that are active in solution state are restricted by the spatial constraint. In consequence, the non-radiative decay channel is blocked, and the excited state energy can be released as photons, leading to greatly enhanced emissions (Mei et al., 2015; Zhao et al., 2015;



Shen et al., 2018). These results confirm that both compounds indeed have AIE properties. And from the fluorescence and phosphorescence spectra of FC6-BP-PXZ and FC6-2BP-PXZ at 77 K (**Figure S2**), the ΔE_{ST} values are estimated to be 0.017 and 0.068 eV, respectively, which are small enough for promoting RISC process.

The transient PL decay spectra show that both FC6-BP-PXZ and FC6-2BP-PXZ have short average lifetimes within 2.0 ns and the delayed fluorescence is hardly observed in solution. However, FC6-BP-PXZ and FC6-2BP-PXZ in neat films show much longer mean lifetimes of 0.22 and 0.62 μ s, with prompt components of 20.7 ns and 29.0 ns and evident delayed components of 0.66 and 2.12 μ s (**Figures 2C,D**), respectively. Moreover, the transient PL decay spectra in water-THF mixtures are further measured. It can be seen that when the water fraction increases, the mean lifetimes become longer. And the ratios of delayed components and the rate constant of RISCs are enhanced greatly (**Table 1, Table S1**). These findings demonstrate that the delayed fluorescence of both compounds is induced by the aggregation formation, indicative of their AIDF nature apparently. In solution state, the excited state is readily deactivated by fast

internal conversion (IC) of vigorous intramolecular motions, and thus the ISC and RISC processes cannot readily occur. In the aggregated state, however, the intramolecular motions are greatly suppressed by spatial hindrance, and the IC channel is blocked. Therefore, given their small ΔE_{ST} values, the ISC and RISC are able to occur, leading to noticeable delayed fluorescence (Guo et al., 2018, 2019).

Theoretical Calculation

The DFT/TDDFT calculation is applied to investigate the molecular orbital amplitude plots and energy levels of the highest occupied molecular orbitals (HOMOs) and lowest unoccupied molecular orbitals (LUMOs) of both compounds. As shown in **Figure 3**, the HOMOs of both compounds are distributed on fluorene and benzoyl moieties, and the LUMOs are concentrated on PXZ. The apparently separated distribution of HOMOs and LUMOs is necessary to achieve small ΔE_{ST} values and thus to promote RISC process and delayed fluorescence. The theoretical ΔE_{ST} values of FC6-BP-PXZ and FC6-2BP-PXZ are calculated to as small as 0.0442 and 0.0422 eV, respectively.

TABLE 1 | Photophysical properties of FC6-BP-PXZ and FC6-2BP-PXZ.

	Solution ^a			Neat film ^b				
	λ_{abs} (nm)	λ_{em} (nm)	$\Phi_{\text{F}}^{\text{c}}$ (%)	λ_{em} (nm)	$\Phi_{\text{F}}^{\text{c}}$ (%)	$\tau_{\text{prompt}}^{\text{d}}$ (ns)	$\tau_{\text{delayed}}^{\text{d}}$ (μs)	$\Delta E_{\text{ST}}^{\text{e}}$ (eV)
FC6-BP-PXZ	317	543	3.5	544	32.0	20.7	0.7	0.017
FC6-2BP-PXZ	330	550	2.0	567	17.0	29.0	2.1	0.068

^aIn THF solution (10^{-5} M) at room temperature. ^bSpin-coated on a quartz substrate. ^cAbsolute fluorescence quantum yield determined by a calibrated integrating sphere under nitrogen at room temperature. ^dPL lifetimes of prompt (τ_{prompt}) and delayed (τ_{delayed}) decay components evaluated at 300 K under vacuum. ^eEstimated from the high-energy onsets of fluorescence and phosphorescence spectra at 77 K.

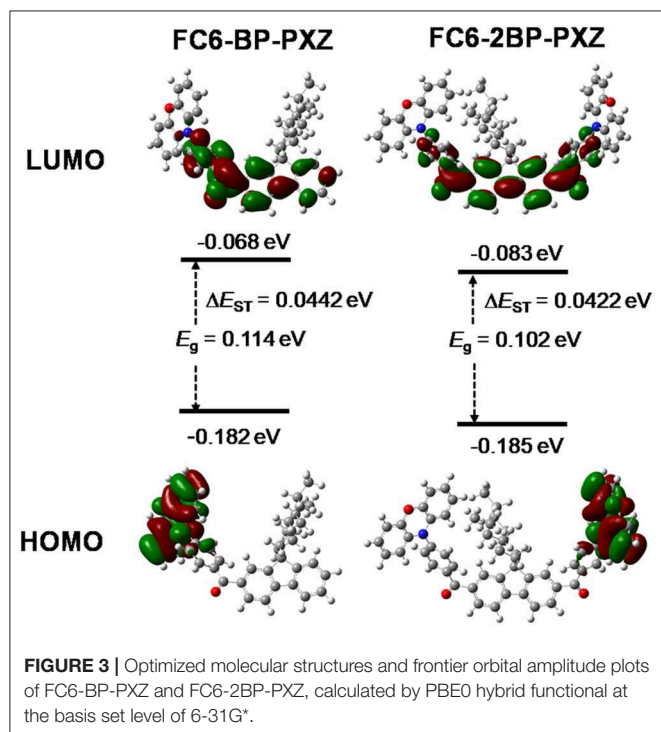


FIGURE 3 | Optimized molecular structures and frontier orbital amplitude plots of FC6-BP-PXZ and FC6-2BP-PXZ, calculated by PBE0 hybrid functional at the basis set level of 6-31G*.

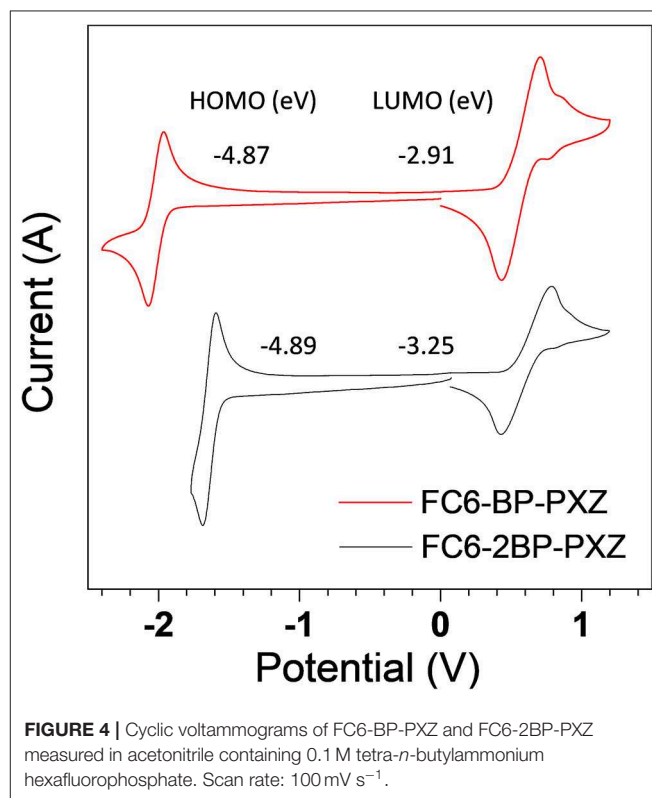


FIGURE 4 | Cyclic voltammograms of FC6-BP-PXZ and FC6-2BP-PXZ measured in acetonitrile containing 0.1 M tetra-*n*-butylammonium hexafluorophosphate. Scan rate: 100 mV s⁻¹.

Electrochemical Property

Cyclic voltammetry (CV) is conducted to investigate the electrochemical behaviors of FC6-BP-PXZ and FC6-2BP-PXZ in a solution of acetonitrile with tetra-*n*-butylammonium hexafluorophosphate (Bu_4NPF_6 , 0.1 M). Three-electrode system (Ag/Ag⁺, platinum wire and glassy carbon electrodes as reference, counter and work electrodes, respectively) is used and the scan rate is 100 mV s⁻¹ in the measurement. As illustrated in **Figure 4**, both compounds undergo reversible oxidation and reduction processes, indicating good electrochemical stability. The oxidation peaks of FC6-BP-PXZ and FC6-2BP-PXZ are both located at 0.435 V and the reduction peaks at -1.96 and -1.60 V, respectively. The HOMO energy levels of FC6-BP-PXZ and FC6-2BP-PXZ are calculated to be -4.87 to -4.89 eV, respectively, from the onset oxidation potentials, and the LUMO energy levels are -2.91 to -3.25 eV, from the onset reduction potentials (HOMO = $-[E_{\text{ox}} + 4.8]$ eV, and LUMO = $-[E_{\text{re}} + 4.8]$ eV, in which E_{ox} and E_{re} represent the onset oxidation and reduction potentials relative to Fc/Fc⁺, respectively).

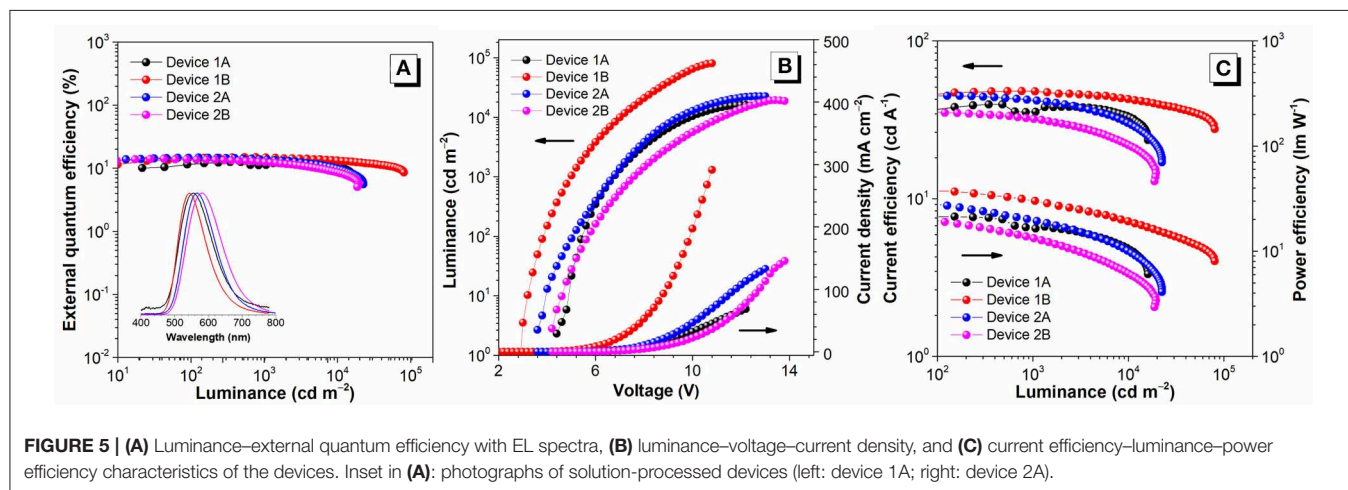
Electroluminescence

Based on the excellent PL properties of FC6-BP-PXZ and FC6-2BP-PXZ, their EL performances in solution-processed OLEDs and vacuum-deposited OLEDs were further investigated. The key data of these OLEDs are summarized in **Table 2**, and the relative characteristic curves are plotted in **Figure 5**. The solution-processed OLEDs with a configuration of ITO/PEDOT:PSS (50 nm)/PVK (30 nm)/emitter/TmPyPB (40 nm)/LiF (1 nm)/Al [Device 1A: emitter = CBP:30 wt% FC6-BP-PXZ (50 nm); Device 2A: emitter = CBP:10 wt% FC6-2BP-PXZ (50 nm)] were fabricated, in which PEDOT:PSS and LiF were used as hole- and electron-injecting layers, respectively; PVK and TmPyPB were selected as hole- and electron-transporting layers, respectively; CBP functioned as a host. As shown in **Figure 5**, the turn-on voltage at 10 cd m⁻² of Devices 1A and 2A are 5.0 and 3.9 V, radiating orange-yellow light at ~ 555 nm (CIE_{x,y} = 0.402, 0.549) and ~ 568 nm (CIE_{x,y} = 0.432, 0.543), respectively. The

TABLE 2 | EL performances of OLEDs based on FC6-BP-PXZ and FC6-2BP-PXZ^a.

	V_{on} (V)	Maximum values					Values at 1,000 $cd\ m^{-2}$					
		η_c ($cd\ A^{-1}$)	η_p ($lm\ W^{-1}$)	η_{ext} (%)	L ($cd\ m^{-2}$)	η_c ($cd\ A^{-1}$)	η_p ($lm\ W^{-1}$)	η_{ext} (%)	RO (%)	λ_{EL} (nm)	CIE (x, y)	
FC6-BP-PXZ	1A	5.0	39.61	21.29	12.49	16100	35.49	16.39	11.20	10.30	555	(0.402, 0.549)
	1B	3.2	48.02	38.91	14.86	80507	47.84	30.06	14.83	0.20	544	(0.392, 0.569)
FC6-2BP-PXZ	2A	3.9	44.83	32.03	14.69	22530	41.76	19.28	13.80	6.06	568	(0.432, 0.543)
	2B	4.6	36.12	25.52	14.12	19455	34.10	31.98	13.22	6.33	582	(0.446, 0.523)

^a V_{on} = turn-on voltage at 10 $cd\ m^{-2}$; η_c = current efficiency; η_p = power efficiency; η_{ext} = external quantum efficiency; RO = current efficiency roll-off from maximum value to that at 1,000 $cd\ m^{-2}$; λ_{EL} = electroluminescence maximum; CIE = Commission Internationale de l'Eclairage coordinates at condition of maximum η_{ext} .



maximum luminance (L_{max}), current efficiency ($\eta_{C,max}$), power efficiency ($\eta_{P,max}$) and external quantum efficiency ($\eta_{ext,max}$) of Device 2A are 22530 $cd\ m^{-2}$, 44.83 $cd\ A^{-1}$, 32.03 $lm\ W^{-1}$, and 14.69%, respectively. It is significant that the external quantum efficiency at luminance of 1,000 $cd\ m^{-2}$ is 13.80%, showing a very low efficiency roll-off of 6.06%. The EL properties of Device 1A is somewhat inferior than those of Device 2A.

To further investigate the EL properties of both compounds, vacuum-deposited OLEDs with a configuration of ITO/TAPC (25 nm)/emitter/TmPyPB (55 nm)/LiF (1 nm)/Al [Device 1B: emitter = CBP:30 wt% FC6-BP-PXZ (35 nm); Device 2B: emitter = CBP: 10 wt% FC6-2BP-PXZ (35 nm)] were fabricated, in which 4,4'-cyclohexylidenebis[N, N-bis(p-tolyl)aniline] (TAPC) and TmPyPB were selected as hole- and electron-transporting layers, respectively. As shown in **Figure 5**, the turn-on voltage at 10 $cd\ m^{-2}$ of Devices 1B and 2B are 3.2 V and 4.6 V, emitting orange-yellow light at ~ 544 nm (CIE_{x,y} = 0.392, 0.569) and ~ 582 nm (CIE_{x,y} = 0.446, 0.523), respectively. The L_{max} , $\eta_{C,max}$, $\eta_{P,max}$, and $\eta_{ext,max}$ of Devices 1B and 2B are 80,507 $cd\ m^{-2}$, 48.02 $cd\ A^{-1}$, 38.91 $lm\ W^{-1}$ and 14.86%, and 19,455 $cd\ m^{-2}$, 36.12 $cd\ A^{-1}$, 25.52 $lm\ W^{-1}$ and 14.12%, respectively, in which the efficiency roll-off is extremely small especially for Device 1B (0.20% at luminance of 1,000 $cd\ m^{-2}$). These new emitters with AIDF property provide good EL performance, and according to the photophysical parameters, the exciton utilization of these OLEDs has approached nearly 100%. More importantly,

extremely small efficiency roll-offs are successfully achieved, which should be an apparent advance to conventional TADF emitters for solution-processed OLEDs and vacuum-deposited OLEDs. And the AIDF character of the materials should be important for achieving high performance, which combines the superior features of efficient solid-state emission, high exciton utilization and low exciton quenching.

CONCLUSIONS

In summary, two new emitters built with electron-withdrawing group benzoyl and electron-donating phenoxazine and 9,9-dihexylfluorene are designed and synthesized. They have high thermal and morphological stabilities and good electrochemical stability. Whereas, in dilute solution state they emit weakly with faint delayed fluorescence, they can emit strongly with prominent delayed fluorescence in the aggregated state, demonstrating the AIDF property. In addition, they fluoresce intensely in spin-coated films with notable delayed fluorescence, owing to the small ΔE_{ST} , and thus fast RISC process. As a consequence, they can perform excellently as light-emitting layers in solution-processed OLEDs, providing high $\eta_{ext,max}$ of up to 14.69% and very small efficiency roll-off at the luminance of 1,000 $cd\ m^{-2}$, demonstrating the outstanding efficiency stability. On the other hand, their vacuum-deposited OLEDs also have good $\eta_{ext,max}$ of up to 14.86% and negligible efficiency roll-off at 1,000 $cd\ m^{-2}$. These results indicate the

great potential of small molecules with AIDF property for the fabrication of high-performance solution-processed and vacuum-deposited OLEDs.

DATA AVAILABILITY STATEMENT

The datasets generated for this study are available on request to the corresponding author.

AUTHOR CONTRIBUTIONS

All authors listed have made a substantial, direct and intellectual contribution to the work, and approved it for publication.

REFERENCES

- Albrecht, K., Matsuoka, K., Fujita, K., and Yamamoto, K. (2015). Carbazole dendrimers as solution-processable thermally activated delayed-fluorescence materials. *Angew. Chem. Int. Ed.* 54, 5677–5682. doi: 10.1002/anie.201500203
- Cho, Y. J., Yook, K. S., and Lee, J. Y. (2014). High efficiency in a solution-processed thermally activated delayed-fluorescence device using a delayed-fluorescence emitting material with improved solubility. *Adv. Mater.* 26, 6642–6646. doi: 10.1002/adma.201402188
- Gather, M. C., Köhnen, A., and Meerholz, K. (2011). White organic light-emitting diodes. *Adv. Mater.* 23, 233–248. doi: 10.1002/adma.201002636
- Gong, S., Fu, Q., Wang, Q., Yang, C., Zhong, C., Qin, J., et al. (2011). Highly efficient deep-blue electrophosphorescence enabled by solution-processed bipolar tetraarylsilane host with both a high triplet energy and a high-lying HOMO level. *Adv. Mater.* 23, 4956–4959. doi: 10.1002/adma.201102758
- Gong, S., Zhong, C., Fu, Q., Ma, D., Qin, J., and Yang, C. (2013). Extension of molecular structure toward solution-processable hosts for efficient blue phosphorescent organic light-emitting diodes. *J. Phys. Chem. C* 117, 549–555. doi: 10.1021/jp309100e
- Guo, J., Fan, J., Lin, L., Zeng, J., Liu, H., Wang, C. K., et al. (2019). Mechanical insights into aggregation-induced delayed fluorescence materials with anti-kasha behavior. *Adv. Sci.* 6:1801629. doi: 10.1002/advs.201801629
- Guo, J., Zhao, Z., and Tang, B. Z. (2018). Purely organic materials with aggregation-induced delayed fluorescence for efficient nondoped OLEDs. *Adv. Opt. Mater.* 6:1800264. doi: 10.1002/adom.201800264
- Higginbotham, H. F., Yi, C. L., Monkman, A. P., and Wong, K. T. (2018). Effects of ortho-phenyl substitution on the rISC rate of D–A type TADF molecules. *J. Phys. Chem. C* 122, 7627–7634. doi: 10.1021/acs.jpcc.8b01579
- Hirata, S., Sakai, Y., Masui, K., Tanaka, H., Lee, S. Y., Nomura, H., et al. (2015). Highly efficient blue electroluminescence based on thermally activated delayed fluorescence. *Nat. Mater.* 14, 330–336. doi: 10.1038/nmat4154
- Huang, J., Nie, H., Zeng, J., Zhuang, Z., Gan, S., Cai, Y., et al. (2017). Highly efficient nondoped OLEDs with negligible efficiency roll-off fabricated from aggregation-induced delayed fluorescence luminogens. *Angew. Chem. Int. Ed.* 56, 12971–12976. doi: 10.1002/anie.201706752
- Kang, Y., Zhao, L., and Leng, J. (2018). Delocalization of frontier orbitals induced red emission for heptazine based thermally activated delayed fluorescence molecule: first-principles study. *Chem. Phys. Lett.* 698, 187–194. doi: 10.1016/j.cplett.2018.03.017
- Kashihara, R., Morimoto, M., Ito, S., Miyasaka, H., and Irie, M. (2017). Fluorescence photoswitching of a diarylethene by irradiation with single-wavelength visible light. *J. Am. Chem. Soc.* 139, 16498–16501. doi: 10.1021/jacs.7b10697
- Kim, H. J., Lee, C., Godumala, M., Choi, S., Park, S. Y., Cho, M. J., et al. (2018). Solution-processed thermally activated delayed fluorescence organic light-emitting diodes using a new polymeric emitter containing non-conjugated cyclohexane units. *Polym. Chem.* 9, 1318–1326. doi: 10.1039/C7PY02113E
- Lee, S. Y., Yasuda, T., Komiya, H., Lee, J., and Adachi, C. (2016). Thermally activated delayed fluorescence polymers for efficient

FUNDING

This work was financially supported by the National Natural Science Foundation of China (21788102 and 21673082), the Natural Science Foundation of Guangdong Province (2019B030301003), the Science and Technology Program of Guangzhou (201804020027).

SUPPLEMENTARY MATERIAL

The Supplementary Material for this article can be found online at: <https://www.frontiersin.org/articles/10.3389/fchem.2020.00193/full#supplementary-material>

- solution-processed organic light-emitting diodes. *Adv. Mater.* 28, 4019–4024. doi: 10.1002/adma.201505026
- Mei, J., Leung, N. L., Kwok, R. T., Lam, J. W., and Tang, B. Z. (2015). Aggregation-induced emission: together we shine, united we soar! *Chem. Rev.* 115, 11718–11940. doi: 10.1021/acs.chemrev.5b00263
- Rajamalli, P., Senthilkumar, N., Gandeepan, P., Huang, P. Y., Huang, M. J., Ren-Wu, C. Z., et al. (2016). A new molecular design based on thermally activated delayed fluorescence for highly efficient organic light emitting diodes. *J. Am. Chem. Soc.* 138, 628–634. doi: 10.1021/jacs.5b10950
- Rajamalli, P., Senthilkumar, N., Huang, P. Y., Ren-Wu, C. C., Lin, H. W., and Cheng, C. H. (2017). New molecular design concurrently providing superior pure blue, thermally activated delayed fluorescence and optical out-coupling efficiencies. *J. Am. Chem. Soc.* 139, 10948–10951. doi: 10.1021/jacs.7b03848
- Shao, S., Hu, J., Wang, X., Wang, L., Jing, X., and Wang, F. (2017). Blue thermally activated delayed fluorescence polymers with nonconjugated backbone and through-space charge transfer effect. *J. Am. Chem. Soc.* 139, 17739–17742. doi: 10.1021/jacs.7b10257
- Shen, P., Zhuang, Z., Zhao, Z., and Tang, B. Z. (2018). AIEgens based on main group heterocycles. *J. Mater. Chem. C* 6, 11835–11852. doi: 10.1039/C8TC02956C
- Suzuki, Y., Zhang, Q., and Adachi, C. (2015). A solution-processable host material of 1, 3-bis [3-(9-carbazolyl) phenyl]-9-carbazolyl benzene and its application in organic light-emitting diodes employing thermally activated delayed fluorescence. *J. Mater. Chem. C* 3, 1700–1706. doi: 10.1039/C4TC02211D
- Thorat, K. G., Ray, A. K., and Sekar, N. (2017). Modulating TICT to ICT characteristics of acid switchable red emitting boradiazaindacene chromophores: perspectives from synthesis, photophysical, hyperpolarizability and TD-DFT studies. *Dyes. Pigm.* 136, 321–334. doi: 10.1016/j.dyepig.2016.08.049
- Uoyama, H., Goushi, K., Shizu, K., Nomura, H., and Adachi, C. (2012). Highly efficient organic light-emitting diodes from delayed fluorescence. *Nature* 492, 234–238. doi: 10.1038/nature11687
- Wu, H., Ying, L., Yang, W., and Cao, Y. (2009). Progress and perspective of polymer white light-emitting devices and materials. *Chem. Soc. Rev.* 38, 3391–3400. doi: 10.1039/b816352a
- Xie, G., Luo, J., Huang, M., Chen, T., Wu, K., Gong, S., et al. (2017). Inheriting the characteristics of TADF small molecule by side-chain engineering strategy to enable bluish-green polymers with high PLQYs up to 74% and external quantum efficiency over 16% in light-emitting diodes. *Adv. Mater.* 29:1604223. doi: 10.1002/adma.201604223
- Yang, X., Guo, H., Liu, B., Zhao, J., Zhou, G., Wu, Z., et al. (2018). Diarylboron-based asymmetric red-emitting Ir (III) complex for solution-processed phosphorescent organic light-emitting diode with external quantum efficiency above 28%. *Adv. Sci.* 5:1701067. doi: 10.1002/advs.201701067
- Zeng, W., Zhou, T., Ning, W., Zhong, C., He, J., Gong, S., et al. (2019). Realizing 22.5% external quantum efficiency for solution-processed thermally activated delayed-fluorescence OLEDs with red emission at 622 nm via a synergistic strategy of molecular engineering and host selection. *Adv. Mater.* 31:1901404. doi: 10.1002/adma.201901404

- Zhao, Z., He, B., and Tang, B. Z. (2015). Aggregation-induced emission of siloles. *Chem. Sci.* 6, 5347–5365. doi: 10.1039/C5SC01946J
- Zhao, Z., Li, J. H., Chen, X., Wang, X., Lu, P., and Yang, Y. (2009). Solution-processable stiff dendrimers: synthesis, photophysics, film morphology, and electroluminescence. *J. Org. Chem.* 74, 383–395. doi: 10.1021/jo802237c
- Zhao, Z., Li, J. H., Lu, P., and Yang, Y. (2007). Fluorescent, carrier-trapping dopants for highly efficient single-layer polyfluorene LEDs. *Adv. Fun. Mater.* 17, 2203–2210. doi: 10.1002/adfm.200700195
- Zhong, P. L., Zheng, C. J., Zhang, M., Zhao, J. W., Yang, H. Y., He, Z. Y., et al. (2020). Highly efficient ternary polymer-based solution-processable exciplex with over 20% external quantum efficiency in organic light-emitting diode. *Org. Electron.* 76:105449. doi: 10.1016/j.orgel.2019.105449
- Zou, Y., Gong, S., Xie, G., and Yang, C. (2018). Design strategy for solution-processable thermally activated delayed fluorescence emitters and their applications in organic light-emitting diodes. *Adv. Opt. Mater.* 6:1800568. doi: 10.1002/adom.201800568

Conflict of Interest: The authors declare that the research was conducted in the absence of any commercial or financial relationships that could be construed as a potential conflict of interest.

Copyright © 2020 Cai, Chen, Guo, Zhao and Tang. This is an open-access article distributed under the terms of the Creative Commons Attribution License (CC BY). The use, distribution or reproduction in other forums is permitted, provided the original author(s) and the copyright owner(s) are credited and that the original publication in this journal is cited, in accordance with accepted academic practice. No use, distribution or reproduction is permitted which does not comply with these terms.